Anti-Platelet Effect Induced by Iron Oxide Nanoparticles: Correlation with Conformational Change in Fibrinogen

Regina Komal Kottana, Lionel Maurizi, Brian Schnoor, Kenise Morris, Jessica Ann Webb, Michael Anthony Massiah, Nadine Millot, Anne-laure Papa

Anti-platelet effect induced by iron oxide nanoparticles: correlation with conformational change in fibrinogen

*Regina Komal Kottana, Lionel Maurizi, Brian Schnoor, Kenise Morris, Jessica Ann Webb, Michael Anthony Massiah, Nadine Millot, Anne-Laure Papa**

R. K. Kottana, B. Schnoor, K. Morris, Prof. A.L. Papa
Department of Biomedical Engineering, School of Engineering and Applied Science, The George Washington University, Washington, DC 20052, USA.
E-mail: alpapa@gwu.edu

Dr. L. Maurizi, Prof. N. Millot
Laboratory ICB, Université Bourgogne Franche-Comté, 9 Avenue Alain Savary, F-21078 Dijon, France.

J. A. Webb, Prof. M. A. Massiah
Department of Chemistry, Columbian College of Arts and Sciences, The George Washington University, Washington, DC 20052, USA.

Keywords: platelets; superparamagnetic iron oxide nanoparticles; polyvinyl alcohol; anti-platelet effect, nanoparticle-protein interactions

Iron oxide nanoparticles have been developed for various biomedical applications, however, there is limited understanding regarding their effects and toxicity on blood components. The particles traveling in circulation inevitably interact with blood cells and plasma proteins and may interfere with hemostasis. Specifically, this study focuses on the influence of superparamagnetic iron oxide nanoparticles (SPIONs) coated with a biocompatible polymer, polyvinyl alcohol (PVA), on platelet function. Here, engineered SPIONs are functionalized with various PVA coatings that provide these particles with different surface charges and polymer packing are described. These formulations are assessed for any interference with human platelet functions and coagulation, *ex vivo*. Positively charged SPIONs induced a significant change in platelet GPIIb-IIIa conformation, indicative of platelet activation at the dose of 500 $\mu g.mL^{-1}$. Remarkably, engineered PVA(polyvinyl alcohol)-SPIONs all display a robust dose-dependent anti-platelet effect on platelet aggregation, regardless of the PVA charge and molecular weight. After assessing hypotheses involving SPION-induced steric hindrance in platelet-platelet bridging, as well as protein corona involvement in the antiplatelet effect, our study concludes that the presence of PVA-SPIONs induces fibrinogen

conformational change, which correlates with the observed dose-dependent anti-platelet effect.

1. Introduction

Engineered superparamagnetic iron oxide nanoparticles (SPIONs) have been used and studied for numerous clinical and potential biomedical applications, such as contrast agents for MRI,[1–4] drug delivery systems,[4–8] hyperthermia inducers,[9,10] and as radiation sensitizers.[11] These particles are also of great interest for industrial applications where they are used as components for magnetic data storage,[12] pigments,[13] catalyst,[14,15] as well as gas sensing.[16,17] Furthermore, iron oxide nanoparticles are also a by-product of fuel combustion, which significantly contributes to their release in the environment as air pollutants.[18,19]

Irrespective of the origin of superparamagnetic iron oxide nanoparticles, the lack of understanding of their effects on physiology is a source of concern. With their increasing utilization, it is important to assess the effects and unintended consequences related to their exposure. Specifically, it is be important to evaluate their interactions with components of the bloodstream. While studies have investigated the intravenous biodistribution and clearance of SPIONs, only a few studies have focused on the effect of SPIONs on hemostasis.[20,21] After their interaction with blood components, nanoparticles undergo spontaneous coating by plasma proteins: the protein corona adsorption.[22–24] The protein corona subsequently affects nanoparticle biodistribution, interaction with the endothelium, and interaction with immune cells.[25,26] Among blood cells, platelets are the main contributors to hemostasis and represent a catalytic surface for the coagulation cascade. Blood proteins such as von Willebrand Factor (vWF), fibrinogen and Factor XII, that are key players during platelet aggregation and/or the coagulation cascade have been detected in the corona of nanoparticles [27,28], including SPIONs' corona.[29,30] Any influence on platelets can have significant consequences, such as aberrant platelet activation that can lead to thrombus formation. Meanwhile, inhibition of platelets can profoundly affect wound healing and normal hemostasis in response to injury.

Thus, it is critical to understand whether SPIONs significantly affect the physiology of platelets, which play a critical role in maintaining the intravascular compartment and are the first responders during vascular injury.

The present study investigates platelet response in the presence of a range of concentrations of SPIONs that have been functionalized with polyvinyl alcohol (PVA) with various molecular weights (M.W.), as well as various end groups to provide these nanoparticles with varying surface chemistry and surface charge. We observed that SPIONs cause a dose-dependent inhibition of platelet aggregation that was attributed to the interaction of PVA-SPIONs with fibrinogen, leading to a change in conformation of the plasma protein. This structural change could impair the ability of fibrinogen to bridge/aggregate platelets.

2. Results

2.1. Characterization of SPIONs and PVA-SPIONs

The bare SPIONs synthesized by co-precipitation displayed a size distribution centered around 23 ± 7 nm as measured by DLS at pH 4 **(Table 1)**. Transmission electron micrographs showed an average crystallite size around 8 nm (**Figure 1 and S1**). Under physiological conditions, bare SPIONs agglomerate to reach a size distribution of 1,930 nm. Following their coating with 12 and 31 kDa PVAs, the surface modified SPIONs exhibited similar size distributions (from 68 ± 22 nm to 88 ± 30 nm) proving their stability under physiological conditions. PVA-SPIONs have varying surface charges as measured by zeta potential **(Table 1).**

We first studied the effect of various formulations of PVA-coated SPIONs on both platelet activation and aggregation. Specifically, we kept the hydrodynamic diameter of the nanohybrids comparable and varied the surface charges (negative, neutral, positive) and/or PVA molecular weight (12 *vs.* 31 kDa) **(Table 1)**.

2.2. Effect of PVA-SPIONs on platelet activation

The degree of platelet activation following their incubation with the various PVA-SPIONs' formulations was measured by the detection of FITC-conjugated PAC-1 antibody *via* flow cytometry. PAC-1 specifically binds to the active conformation of platelet glycoprotein GPIIb-IIIa, which is a hallmark of platelet activation. We first carried out a series of experiments in the absence of soluble agonists, to determine whether the PVA-SPIONs themselves would modulate platelet function at baseline. Platelets underwent significant activation solely in the presence of positively charged PVA-SPIONs at 500 $\mu g.mL^{-1}$, and irrespective of the polymer molecular weight, when compared to the control group ($P \leq 0.001$ and $P \leq 0.001$ for 12^+ and 31^+ formulations, respectively) **(Figure 2A-C)**. At 50 $\mu g.mL^{-1}$ dose, PAC-1 binding was similar to the control group ($P=0.880$ and $P=0.989$ for 12^+ and 31^+, respectively). In addition, neutral and negatively charged PVA-SPIONs did not induce platelet activation at baseline either, regardless of the M.W. of PVA **(Figure 2A-C)**. Lastly, PVA-SPIONs did not modulate platelet activation in presence of ADP, regardless of the agonist concentration (20 µM or 50 µM) **(Figure 3A,B)**.

2.3. Effect of PVA-SPIONs on platelet aggregation

To study the effect of PVA-coated SPIONs on platelet aggregation, platelets were incubated with PVA-SPIONs and assessed by light transmission aggregometry in presence of 20 µM ADP. An inhibitory effect was observed when platelets were incubated with 250 $\mu g.mL^{-1}$ SPIONs for 12^+ ($P<0.001$), 12^0 ($P=0.046$) and 31^+ ($P=0.002$), and 500 $\mu g.mL^{-1}$ for 12^+, 12^0, 12^-, 31^+, 31^0 and 31^- as compared to the control ($P<0.001$ for all formulations) **(Figure 4)**. This effect was non-significant at lower doses of SPIONs, *i.e.* 50 and 100 $\mu g.mL^{-1}$, when compared to the control **(Figure 4)**. Additionally, a dose effect was observed in the aggregation percentage when the different concentrations were compared to each other. There was a significant decrease in aggregation when the dose was increased from 50 $\mu g.mL^{-1}$ to 500 $\mu g.mL^{-1}$ ($P < 0.001$ for all formulations). Similarly, the same trend is shown for the dose of 50 $\mu g.mL^{-1}$ when compared to 250 $\mu g.mL^{-1}$ ($P=0.008$ for 12^0, $P=0.039$ for 12^-, and $P=0.16$

for 31^0), and 100 µg.mL^{-1} when compared to 500 µg.mL^{-1} ($P<0.001$ for 12^+, 12^0, 12^-, and 31^-, $P=0.004$ for 31^0) **(Figure 4)**. Because the 12 PVA-SPIONs and 31 PVA-SPIONs seem to have very similar effects on platelet functions, we conducted the remaining experiments of the study utilizing 12^+, 12^0 and 12^- PVA-SPIONs only.

2.4. Fibrinogen and vWF adsorption on PVA-SPIONs

Next, the levels of fibrinogen and vWF, two plasma proteins implicated in platelet aggregation, were evaluated with and without SPIONs' incubation. The goal was to assess whether these proteins would be adsorbed at the surface of the SPIONs (within their protein corona) to the extent that this could significantly deplete these proteins from plasma and potentially affect platelet aggregation. A one-way ANOVA and Dunnett's multiple comparison analysis showed no significant difference among groups **(Figure 5A,B)**.

2.5. Steric Effects of PVA-SPIONs on Fibrinogen and vWF

We investigated whether a steric hindrance provided by particles in the platelet suspensions could affect fibrinogen and vWF binding to platelets, and thus indirectly impair platelet aggregation. An AF647-conjugated human fibrinogen was used to characterize fibrinogen binding to washed platelets in presence of the SPIONs *versus* control (no SPIONs) by flow cytometry. Data indicated a trend with increased binding of fibrinogen to platelets solely for the 12^+ PVA-SPIONs with a significant effect at high concentration, *i.e.* 500 µg.mL^{-1} ($P<0.0001$) **(Figure 6A,B)**. Fibrinogen binding to platelets was similar in control and in platelet suspension supplemented with 12^0 PVA-SPIONs and 12^- PVA-SPIONs, regardless of the concentration **(Figure 6A,B)**.

The steric effect of SPIONs on vWF was assessed using an AF488-conjugated anti-human vWF antibody to determine the availability of vWF bound to the surface of the platelets. This was used to assess if the presence of SPIONs prevented the binding of the antibody to the vWF on the platelet surface. The detection of vWF on the platelet surface using this antibody thus provides an indication of if the protein is available to form bridges

between activated platelets and thus promote aggregation. The detection of vWF on the platelet surface was similar with or without PVA-SPIONs, regardless of the surface charge and concentration (comparisons *versus* control: P = ns for all conditions) **(Figure 6C,D)**.

2.6. Fibrinogen conformational change in the presence of PVA-SPIONs

We then hypothesized that even though fibrinogen could bind the GPIIb-IIIa platelet receptor, a change in conformation due to the presence of the PVA-SPIONs would impair bridging, and thus, platelet aggregation. Our UV-visible data demonstrates a decrease in the maximum absorbance peak of human fibrinogen at 204.4 nm ($P<0.001$, $P<0.001$ and $P<0.001$ for 12^+, 12^0 and 12^- at 50 $\mu g.mL^{-1}$ respectively) when the protein is incubated with PVA-SPIONs. We also observed a right shift of ~2.97 nm of the maximum absorbance peak (λ_{max}) ($P<0.001$ for 12^+, 12^0 and 12^- at 50 $\mu g.mL^{-1}$) **(Figure 7A-C)**. The addition of PVA controls (12^+, 12^0 and 12^-) to fibrinogen did not demonstrate a significant change in the protein absorbance spectrum (shift in peak wavelength: $P=0.902$, $P>0.999$ and $P>0.999$ and λ_{max}: $P>0.999$, $P=0.653$ and $P=0.918$ for PVA controls 12^+, 12^0 and 12^-). However, the bare SPION control had a reduction in fibrinogen absorbance compared to the absorbance of the fibrinogen control ($P=0.010$ at 50 $\mu g.mL^{-1}$). To validate these results, we assessed changes in the intrinsic fluorescence of the amino acids tryptophan (Trp) and tyrosine (Tyr) through steady state fluorescence spectroscopy[31]. Tryptophan's fluorescence was further analyzed by synchronous fluorescence spectroscopy[31]. In **Figure 7D-F**, the steady state fluorescence shows the emission peak of fibrinogen at 345.6 nm. In the presence of the PVA, there was an increase in fluorescence intensity (significant for PVA 12^- only, $P=0.017$). The bare SPIONs, as well as PVA-SPIONs 12^+, 12^0, and 12^- (20 $\mu g.mL^{-1}$) showed a significant decrease in fluorescence intensity ($P<0.001$ for bare SPIONs, 12^+, 12^0 and 12^-). A shift in peak wavelength was observed only in the presence of the 12^0 PVA-SPIONs ($P=0.041$), and a one-way ANOVA and Tukey's multiple comparison analysis showed no significant difference among the other groups (P=ns, for 12^+, 12^-, bare SPIONs, PVA 12^+, PVA 12^0, and PVA 12^-).

Synchronous fluorescence scans the emission and excitation together at a constant offset value, **Δ**λ, which independently measures tryptophan at 60 nm. In **Figure 7G-I**, the synchronous fluorescence spectra show the peak intensity of fibrinogen in the absence and presence of the PVA-SPIONs. Fibrinogen signal underwent a red shift of 1.5 nm in the presence of the 12^{+} PVA-SPIONs (P=0.045). Change in fluorescence intensity was also observed for synchronous fluorescence in the presence of all formulations. There was a significant decrease in maximum fluorescence intensity in the presence of 12^{+} (P=0.004), 12^{0} (P=0.019), 12^{-} (P=0.007), and bare SPIONs (P<0.001) at 20 µg.mL^{-1} respectively. A significant increase in maximum fluorescence intensity was only observed for PVA 12^{-} (P=0.022).

2.7. Coagulation parameters in presence of PVA-SPIONs

The various formulations have also been assessed for their potential modulation of the coagulation cascade, specifically, the prothrombin time (PT) and activated partial thromboplastin time (aPTT). Data analysis showed no significant difference between PVA-SPION treated samples and platelet poor plasma control group for both PT and aPTT **(Figure S2)**.

3. Discussion

We created six formulations of SPIONs stabilized by PVA coating with various polymer molecular weights, as well as net nanohybrid charge. These formulations had surface charge variation as measured by zeta potential, alongside with diverse polymer packing due to the differential lengths of PVA used (12 and 31 kDa). Subsequently, we assessed these negatively charged, neutral and positively charged PVA-SPIONs for their effects on human platelet activation and aggregation, *ex vivo*. We first explored whether these nanohybrids had any effect on platelet activation, in the absence of platelet soluble agonists. Only the 12^{+} PVA-SPION formulation at high concentration (500 µg.mL^{-1}) exerted significant platelet

activation at baseline. Literature suggests that positively charged SPIONs are more likely to closely interact with the cell membrane and get internalized within cells [32], as compared to their neutral and negatively charged counterparts. This could explain that, in our study, the interacting positively charged SPIONs triggered an activation signalling pathway at the level of the platelet membrane, as opposed to the absence of this effect seen with neutral and negatively charged nanoparticles. However, normal platelet activation triggered by 20µM ADP remained unaltered in the presence of PVA-SPIONs, regardless of the studied formulation.

This suggests that the PVA-SPIONs do not impair the platelet response to agonist induced activation and do not alter platelet signalling pathways, even at a high dose of nanoparticles. However, the ADP response at 20µM could already be maximal, which might be a limitation on the sensitivity of this assessment. Lower concentrations were not investigated because of insufficient platelet activation at the tested concentrations.

Next, we observed a significant inhibitory effect of platelet aggregation which was dose dependent. The effect was seen regardless of the PVA molecular weight or the net charge of these PVA-SPION formulations. In literature, the main focus related to SPIONs' effect on hemostasis has been on their modulation of the coagulation parameters, rather than on platelet function. Indeed, bare 22 nm SPIONs induced a significant increase in prothrombin time (PT) and activated partial thromboplastin time (aPTT) following 0.8mg.kg^{-1} intratracheal instillation in rats [21]. SPIONs coated with P4VP-g-PEG copolymer significantly enhanced aPTT as well, while having no effect on PT [20]. In the current study, PVA-coated SPIONs have no effect on either aPTT and PT as well. These variable results suggest that, even though the core of nanoparticles might be of similar composition/size, the nature and density of the surface coating significantly affect the nature and packing of the nanoparticle's corona, as highlighted in the review by Lee *et al*.[33], which subsequently might affect clotting factors/time. Regarding platelet function, bare SPIONs have been reported to promote

thrombosis and thus, platelet activation/aggregation [34]. Other SPION formulations have no influence on platelet functions [35,36]. Specifically, counterpart 30 nm carbon-coated iron–carbide nanomagnets do not influence normal platelet aggregation with tested nanomagnet concentrations below 1 $mg.mL^{-1}$, whether or not they are coated with PEG [35]. Hyaluronic acid- and chitosan-modified iron oxide nanoparticles did not affect platelet aggregation up to 1 $mg_{Fe}.mL^{-1}$, while polyacrylic acid- modified iron oxide nanoparticles did induce significant platelet aggregation at this concentration.[36]

We then hypothesized that the observed anti-platelet effect could independently or concomitantly be attributed to (i) the trapping of fibrinogen and/or vWF in the protein corona of PVA-SPIONs which would significantly reduce the availability of these bridging plasma proteins for platelet aggregation, (ii) steric hindrance due to the presence of the SPIONs in the platelet suspensions thus interfering with platelet bridging (*i.e.* platelet aggregation) following their activation, and (iii) conformational change of fibrinogen in the presence of the SPIONs, thus impairing platelet bridging and subsequent aggregation **(Figure 8)**. Indeed, fibrinogen and vWF have been detected in the adsorbed plasma protein corona of SPIONs [30] and our SPIONs have a high specific surface area (~150 $m^2.g^{-1}$) to support protein adsorption. However, our data does not support the adsorption of plasma proteins as being a significant parameter affecting fibrinogen and vWF concentration in our platelet poor plasma samples. Next, the significant GPIIb-IIIa receptor activation observed with 12^+ PVA-SPIONs at 500 $\mu g.mL^{-1}$ **(Figure 2C)** would in theory, indicate an increased affinity of the receptor for fibrinogen [37]. This was corroborated with a significantly greater fibrinogen binding **(Figure 6A)** seen with these positively charged nanoparticles as well. Importantly, PVA-SPIONs did not impair fibrinogen binding to platelets, regardless of the formulations (*i.e.* charge and PVA M.W.). Additionally, no PVA-SPION formulations had an observable steric effect preventing the antibodies from binding to vWF on the platelet surface. However, the SPIONs did impact human fibrinogen structure as observed *via* UV-visible spectroscopy and intrinsic tryptophan

fluorescence. The red shift contribution of the maximum absorbance change of fibrinogen in the presence of the various PVA-SPION formulations suggested a change in fibrinogen conformation and/or an interaction between fibrinogen and the SPIONs. The change in conformation was confirmed by a significant decrease in fibrinogen's tryptophan fluorescence as well. The microenvironment of tryptophan can be affected by a change of exposure to solvent and the presence of other amino acids in close proximity most commonly caused by conformational changes[38]. A blue shift suggests that tryptophan side chains became more buried in a hydrophobic environment while the red shift suggests tryptophan became exposed to solvent[39].

Bare iron oxide nanoparticles are known Förster resonance energy transfer (FRET) acceptors for tryptophan (donor), and thus, are able to quench its fluorescence[40]. This can explain the large quenching effect observed with uncoated-SPIONs in our experiments. However, the PVA coating on the surface of SPIONs prevents close interaction between the FRET donor (Trp) and acceptor (SPIONs). A FRET effect in this experimental scenario would be highly unlikely considering the thickness of the PVA layer at the SPION surface observed from the increase of DLS sizes after PVA coatings (Table 1), and estimated to be at least bigger than 10 to 15 nm for each type of PVA-SPIONs. These PVA-layer thicknesses in physiological conditions are in accordance with previous studies on other SPIONs also functionalized with PVA (10 nm thickness[41–43]). Because FRET only occurs when the donor and acceptor are in direct proximity (< 10 nm[44]), we thus ascribed the significant fluorescence quenching of tryptophan in the presence of PVA-SPIONs to a conformational change in fibrinogen.

In addition, our data indicates that fibrinogenesis is not impacted by PVA-SPIONs, as highlighted by similar clotting times in the presence of the particles compared to the plasma control. Thus, this suggests that the cleavage site would be readily available to thrombin and would support our spectrometric data highlighting a conformational change in fibrinogen, rather than its aggregation. This is also supported by literature demonstrating that

nanoparticles indeed can affect fibrinogen conformation [45–50], including iron oxide nanoparticles [31]. Accordingly, Zhang *et al.* reported that UV-vis spectroscopy of bovine fibrinogen incubated with 10 nm γ-Fe_2O_3 indicated a decrease in absorbance intensity in the peaks at 218 nm and 275 nm when compared to fibrinogen[31]. In agreement with our data, a significant reduction in the intrinsic fluorescence of fibrinogen's tryptophan in steady state and synchronous conditions was also observed[31].

Taken together, our data demonstrates that fibrinogen is able to bind to platelets, with a failure of bridging due to conformational change in the presence of the PVA-SPIONs.

4. Conclusion

In conclusion, we demonstrated an "antagonistic" effect on platelet activation and aggregation observed with positively charged PVA-SPIONs. These particles activate but do not aggregate platelets in absence of platelet agonists. Physiologically, platelet activation is a precursor to platelet aggregation. Thus, our results would indicate that (i) this coherence is lost in the presence of positively charged PVA-SPIONs and (ii) the impairment is first triggered by an external factor, as platelet activation normally leads to their aggregation. All formulations (positively, neutral and negatively charged particles) did not induce steric hindrance between fibrinogen and platelets; however, they impact fibrinogen structure, coupled with their inhibitory effect on platelet aggregation. Our study combined with existing literature would suggest that nanoparticles could affect plasma protein conformation. Such effects could have implications beyond physiological platelet function and impact the coagulation cascade or the immune response. Thus, further studies are required to fully comprehend the various implications of the interactions of nanomedicines (or even environmental pollutants) with blood components.

5. Experimental Section/Methods

Materials: Iron (II) chloride tetrahydrate ($FeCl_2$, $4H_2O$ 98%), iron (III) chloride hexahydrate ($FeCl_3$, $6H_2O$, 98%), ferric nitrate ($Fe(NO_3)_3$ 98%), ammonium hydroxide (NH_4OH, 28%),

hydrochloric acid (HCl, 37%), nitric acid (HNO_3, 65%), sodium chloride (NaCl, 99%), and polyvinyl alcohol (PVA; Mowiol 4-88) with a hydrolysis degree of 88% and an average molecular weight of 31 kDa (PVA-31) were purchased from Sigma Aldrich and used without any further purification. PVA (Mowiol 3-85) with a hydrolysis degree of 85% and an average molecular weight between 12 and 14 kDa (PVA-12) and carboxylic acid functionalized PVA (KL-506) with randomly distributed carboxylic acid groups, with a hydrolysis degree of 74–80% and an average M.W. of 30,000 – 50,000 $g.mol^{-1}$ (PVA-COOH), were supplied by Kuraray Europe GmbH. Polyvinyl alcohol/vinyl amine (PVA-NH_2) copolymer M12 with an average M.W. of 80,000 – 140,000 was supplied by Erkol. Adenosine diphosphate (ADP) (P/N 384) has been purchased at Chrono-log Corporation. FITC mouse IgM,k isotype control (cat# 551448) and FITC mouse anti-human PAC-1 (cat# 340507) were obtained from BD Biosciences. AF647-conjugated human fibrinogen (cat# F35200) and human fibrinogen (cat# RP-43142) were purchased from Invitrogen. AF488-conjugated mouse anti-human vWF (cat# NBP2-34535AF488) and AF488-conjugated mouse IgG1 isotype control (cat# IC002G) were obtained from Novus Biological. Phospholin ES (Catalog # 21-405) and Phosphoplastin RL (Catalog # 11-305) were purchased from r^2 Diagnostics, Inc. Chemical solutions were prepared in deionized water (DI water).

Synthesis and functionalization of SPIONs: SPIONs were synthesized following a classical alkaline co-precipitation method. Briefly, a 150 mL solution with a molar ratio of 1 iron (II) with 2 iron (III) at 6.4 mM and 12.8 mM respectively was mixed with 12 mL of NH_4OH. After 5 minutes of co-precipitation, the suspension of SPIONs was washed five times with DI water and by magnetic decantation before being dialyzed against HNO_3 10 mM for 48 hours, while replacing the dialysis solution every 12 hours. After dialysis, the SPIONs were centrifuged at 20,000 g for 15 min to remove large aggregates. The final concentration was adjusted at 10 mg $_{SPIONs}.mL^{-1}$ with HNO_3 10 mM.

Bare SPIONs were then functionalized with several PVAs at different concentrations in order to stabilize them and to provide different surface chemical groups and charges. PVA-COOH and PVA-NH_2 were chosen to add negative and positive charges to SPIONs, respectively. The functionalization process was optimized from previous studies [30,51]. Solutions of PVA-12, PVA-31 and PVA-COOH at 100 mg $_{PVA}$.mL^{-1} were prepared and filtered in ultrapure water. 20 mg_{PVA}.mL^{-1} of PVA-NH_2 were also dissolved in the same conditions. Six suspensions of 10 mL of PVA functionalized SPIONs at a final concentration of 5 mg $_{SPIONs}$.mL^{-1} were obtained by mixing different volumes of the PVA solutions and water with a constant volume of naked SPIONs. The volumes and mass ratios used as well as the chemical groups added on the SPIONs' surface are given in **Table 1**.

The SPION suspensions were adjusted to physiological pH prior to further characterization.

Size distribution and zeta potential of PVA-SPIONs: The hydrodynamic diameters and the zeta potentials of the various PVA-SPIONs were analysed utilizing a Zetasizer NanoZS (Malvern Instruments Inc., UK). This was done with the Zetasizer Nano software v7.2. The nanoparticle suspensions were diluted at a 1:25 ratio in 0.15 M NaCl at pH 7.4 for DLS measurements and in 10 mM NaCl at pH 7.4 for zeta potential measurements. The hydrodynamic sizes were given weighted in number.

Transmission Electron Microscopy (TEM): The suspension of SPIONs was diluted at a 1:10 ratio in DI water and a 20 µL droplet was added to a copper grid before analyses by TEM using a JEOL JEM – 2100F instrument with an acceleration voltage of 200 kV and a resolution of 0.19 nm. Average crystallite diameter was obtained by counting the diameters of 200 nanoparticles **(Figure S1)**.

Specific surface area: Specific surface area of bare SPIONs was measured on a sorptometer 3020 from Tristar under nitrogen. The sample was degassed 15 hours at 100°C before the measurement.

Absorbance curves of PVA-SPIONs: To determine the interference of the PVA-SPIONs due to absorbance during the Light Transmission Aggregometry study, the SPIONs were diluted at concentrations of 50 $\mu g.mL^{-1}$, 100 $\mu g.mL^{-1}$, 250 $\mu g.mL^{-1}$ and 500 $\mu g.mL^{-1}$ in PBS (phosphate buffered saline). 100 µL of these suspensions was then plated in a 96-well plate and the absorbance spectra was recorded from 600 nm to 1,000 nm with the SpectraMax iD5 (Molecular Devices).

Human Blood Platelet Isolation: Healthy human blood was commercially sourced from BioIVT, NY, following approval from the Institutional Biosafety Committee at the George Washington University. Blood was collected and shipped overnight before being used in our experiment (within 15-20 hours of collection). Whole Blood collected with 3.8% sodium citrate was centrifuged at 150 g for 20 min and the Platelet Rich Plasma (PRP) was collected. Post collection of the PRP, the remaining blood fraction was centrifuged at 2,000 g for 20 min to obtain Platelet Poor Plasma (PPP). For Flow cytometry analysis, PRP was diluted to $0.1x10^6$ platelets/µL with Tyrode buffer (136 mM NaCl, 12 mM $NaHCO_3$, 2.9 mM KCl, 0.34 mM Na_2HPO_4, 1 mM $MgCl_2$ and 10 mM HEPES buffer). For Light Transmission Aggregometry (LTA), PRP was diluted at $0.2x10^6$ platelets/µL with PPP. PPP was stored at -80°C before performing ELISA (enzyme-linked immunosorbent assays).

Platelet activation by flow cytometry: Platelets ($0.1x10^6$ platelets/µL) were incubated with SPIONs at concentrations of 50 $\mu g.mL^{-1}$ and 500 $\mu g.mL^{-1}$ for 10 min at room temperature. They were then incubated with ADP at 20 µM and 50 µM for 10 min. Subsequently, the samples were incubated with FITC-conjugated mouse anti-human PAC-1 antibody for 20 min. PAC-1 antibody selectively binds to the active conformation of the glycoprotein GPIIb-IIIa on the platelet surface, thus indicating platelet activation. FITC-conjugated mouse IgM,k isotype was used as a control for non-specific binding. 2% paraformaldehyde was used as fixative. The samples were then analyzed using the Novocyte flow cytometer (ACEA Biosciences Inc.).

Platelet aggregation by Light Transmission Aggregometry (LTA): PRP was incubated with SPIONs at concentrations of 50 µg.mL^{-1}, 100 µg.mL^{-1}, 250 µg.mL^{-1} and 500 µg.mL^{-1} for 5 min under constant stirring at 1,200 rpm and 37°C. ADP at concentrations of 20 µM and 50 µM was used as the agonist. The samples were run using a Chrono-log Corporation aggregometer (model 490 4 + 4) for 7-8 min. The sample transmittance values over time were recorded at 940 nm. The absorbance spectra for PVA-SPIONs at the concentrations used in these experiments was obtained to ensure that the SPIONs do not interfere with the absorbance at the wavelength utilized by the aggregometer **(Figure S3)**. Measurements were also conducted to detect any variability in the concentration of SPIONs in plasma during the 7-8 min of LTA data acquisition under magnetic stirring **(Figure S4)**.

Quantification of vWF and fibrinogen in plasma (ELISAs): ELISAs were used for the quantification of von-Willebrand Factor (Thermo Fisher, cat# EHVWF) and Fibrinogen (Cell Sciences, cat# CSI20049A) in plasma. 500 µg.mL^{-1} SPIONs were incubated with PPP for 10 min and then these samples were placed on a magnet (EasyStep™ Magnet, Stem Cell Technologies) overnight to separate the SPIONs from plasma. SPION-free plasma samples were then diluted at 1:2,500 and 1:333,000 for the von-Willebrand Factor and the fibrinogen quantification, respectively. The ELISAs were performed according to manufacturer protocols.

Assessment of SPIONs' steric effect on fibrinogen and vWF: PRP was incubated with 1 µM PGE1 for 10 min and centrifuged at 1,000 g for 15 min and the platelet concentrate was obtained. This platelet concentrate was washed once with Tyrode buffer and then resuspended in Tyrode (1x10^6 platelets in 1,000 µL). For the fibrinogen binding study, the washed platelets (0.1x10^6 platelets/µL) were recalcified with 10 µM $CaCl_2$ and then incubated with 50 µg.mL^{-1} and 500 µg.mL^{-1} of SPIONs for 10 min. The platelets in separate aliquots were then incubated with 100 µg.mL^{-1} AF647-conjugated-human fibrinogen for 5 min.

In order to assess the steric effect of SPIONs on vWF, the washed platelets ($0.3x10^6$ platelets/uL) were recalcified with 10 µM $CaCl_2$ and then incubated with 50 $\mu g.mL^{-1}$ and 500 $\mu g.mL^{-1}$ of SPIONs for 10 min. These samples were further diluted with Tyrode to obtain platelet count of $0.1x10^6$ platelets/µL which were then incubated for 20 min with an AF488-conjugated anti-vWF or its corresponding isotype control. For both the studies, the samples were then fixed with 2% paraformaldehyde and flow cytometry analysis was performed.

Absorbance measurements of fibrinogen: To assess the change in structure of the human fibrinogen protein in the presence of SPIONs, absorbance measurements were performed in the UV-visible range. Fibrinogen was diluted to 680 $\mu g.mL^{-1}$ with physiological saline (0.9% NaCl) and incubated with 50$\mu g.mL^{-1}$ of SPIONs for 10 min. The absorbance spectra were recorded from 190 nm to 400 nm with the NanoDrop 2000 (Thermo Fisher Scientific, ThermoScientific™). Optical corrections were performed for samples incubated with SPIONs by subtracting the replicate average of the absorbance signal generated by the SPIONs from the sample signal.

Tryptophan fluorescence measurements: Human fibrinogen's structure was examined with and without the addition of SPIONs by steady state and synchronous fluorescence on HORIBA's FluoroMax-4. 0.5 µM of fibrinogen in PBS was used for all experiments. PVA-SPIONs were added to a final concentration of 20 µg/mL. Fibrinogen was incubated with PVA-SPIONs for 10 minutes prior to experiments at room temperature. Steady-state data were collected at an excitation of 280 nm and the emission ranged from 300 to 500 nm with 1 nm increments. Synchronous spectra were collected between an excitation of 200 and 500 nm with an offset of 60 nm for tryptophan (Trp) residues[31,52,53]. The slit width for all experiments was 4 nm for excitation and emission.

Activated Partial Thromboplastin Time (aPTT) and Prothrombin Time (PT) measurements: aPTT and PT assays were obtained from r^2 Diagnostics, Inc, and used according to manufacturer protocols. Briefly, PPP was incubated with 500 $\mu g.mL^{-1}$ of PVA-SPIONs for 10

min. aPTT was measured manually by incubating 100 µL of PPP (with or without SPIONs) mixed with 100 µL of the Phospholin ES reagent for 5 min at 37°C in a water bath. 100 µL of prewarmed 0.025M $CaCl_2$ was added to induce the clot formation and aPTT time was simultaneously recorded. Similarly, for the PT, the PPP (with or without SPIONs) was incubated for 3 min at 37°C in a water bath. 200 µL of prewarmed Phosphoplastin RL reagent was added to induce clot formation and PT time was measured manually.

Iron concentration determination by ferrozine assay: To determine the decrease in concentration of SPIONs in suspension due to the magnetic stirring during Light Transmission Aggregometry, all formulations of PVA-SPIONs were diluted in PBS at 50 $\mu g.mL^{-1}$ in 300 µL. The suspension was divided into two aliquots: a control and a test sample. The test sample was run in the same condition as the aggregometry experiment. Both the aliquots were analyzed for iron concentration utilizing a ferrozine assay. For the ferrozine assay, 200 µL of 10 mM HCl and 100 µL of iron releasing agent (equal volumes of 4.5% (w/v) 0.285 M $KMnO_4$ and 1.2 N HCl) was added to 100 µL of sample. This mixture was incubated at 60°C for two hours in the dark. After a cooling period of 30 min, 30 µL of the iron chelating (ferrozine) reagent (6.5 mM ferrozine, 13.1 mM neocuproine, 2 M ascorbic acid and 5 M ammonium acetate) was added. 150 µL of the samples were then plated in a 96-well plate and the absorbance measurement was recorded at 562 nm using the SpectraMax iD5 (Molecular Devices).

Statistical analysis: GraphPad Prism software was used to perform statistical analysis. Specifically, the one-way ANOVA test with Tukey's test for multiple group comparison and Dunnett's test for comparison to control was used to determine significances (*$P \leq 0.05$, **$P \leq 0.01$, ***$P \leq 0.001$ and ****$P \leq 0.0001$). All figures display the mean ± SEM for each group.

Supporting Information

Supporting Information is available from the Wiley Online Library or from the author.

Acknowledgements

This work has been supported by the George Washington University startup funds (ALP). We acknowledge support from the Bourgogne Franche-Comté Graduate School EUR-EIPHI (17-EURE-0002) (LM, NM), the ANER project "Nanoprot" n° 2019-Y-10648 (LM) and the European Union through the PO FEDER-FSE Bourgogne 2014/2020 programs (LM, NM). The authors would like to thank Dr. Zhenyu Li (GWU) for generously giving us access to his laboratory's Thermo Scientific™ NanoDrop 2000 instrument, Dr. Lucien Saviot (UBFC) for his excellent input on spectroscopy data and Dr. Rémi Chassagnon (UBFC) for the TEM images. The graphical abstract and figure 8 were created with BioRender.com.

Author Contributions

Study design: RKK, ALP (conception of study and platelet studies), LM, NM (particle synthesis and characterization), RKK, JW, MAM (tryptophan fluorescence studies). SPION synthesis, functionalization and characterization: LM. Platelet activation and aggregation studies, ferrozine assays, absorbance measurements of SPIONs: RKK. ELISA studies: RKK and KM. Fibrinogen/vWF binding studies: RKK and BS. Absorbance measurements of fibrinogen: RKK and BS. Tryptophan fluorescence studies: RKK, JW and MAM. Authors analyzed the data and prepared figures for their respective experiments. Writing – Original Draft Preparation: RKK and ALP; Writing – Review & Editing: all authors; Funding Acquisition: LM, NM and ALP.

Declaration of interest

The authors declare no competing financial interest.

Received: ((will be filled in by the editorial staff))
Revised: ((will be filled in by the editorial staff))
Published online: ((will be filled in by the editorial staff))

References

[1] L. Li, W. Jiang, K. Luo, H. Song, F. Lan, Y. Wu, Z. Gu, *Theranostics* **2013**, *3*, 595.
[2] Z. Shen, A. Wu, X. Chen, *Mol. Pharm.* **2017**, *14*, 1352.
[3] G. Thomas, J. Boudon, L. Maurizi, M. Moreau, P. Walker, I. Severin, A. Oudot, C. Goze, S. Poty, J.-M. Vrigneaud, F. Demoisson, F. Denat, F. Brunotte, N. Millot, *ACS Omega* **2019**, *4*, 2637.
[4] J. Ward, J. A. Guthrie, M. B. Sheridan, S. Boyes, J. T. Smith, D. Wilson, J. I. Wyatt, D. Treanor, P. J. Robinson, *J. Clin. Oncol.* **2008**, *26*, 4304.
[5] Z. Bakhtiary, A. A. Saei, M. J. Hajipour, M. Raoufi, O. Vermesh, M. Mahmoudi, *Nanomedicine* **2016**, *12*, 287.
[6] T. Bonnard, M. Gauberti, S. Martinez de Lizarrondo, F. Campos, D. Vivien, *Stroke* **2019**, *50*, 1318.
[7] N. Singh, F. Sallem, C. Mirjolet, T. Nury, S. K. Sahoo, N. Millot, R. Kumar, *Nanomaterials (Basel)* **2019**, *9*, DOI 10.3390/nano9020138.
[8] F. Sallem, R. Haji, D. Vervandier-Fasseur, T. Nury, L. Maurizi, J. Boudon, G. Lizard, N. Millot, *Nanomaterials (Basel)* **2019**, *9*, DOI 10.3390/nano9020287.
[9] D. Chang, M. Lim, J. A. C. M. Goos, R. Qiao, Y. Y. Ng, F. M. Mansfeld, M. Jackson, T. P. Davis, M. Kavallaris, *Front Pharmacol* **2018**, *9*, 831.
[10] K. Hayashi, K. Ono, H. Suzuki, M. Sawada, M. Moriya, W. Sakamoto, T. Yogo, *ACS Appl Mater Interfaces* **2010**, *2*, 1903.
[11] A. K. Hauser, M. I. Mitov, E. F. Daley, R. C. McGarry, K. W. Anderson, J. Z. Hilt, *Biomaterials* **2016**, *105*, 127.
[12] S. Singamaneni, V. N. Bliznyuk, C. Binek, E. Y. Tsymbal, *J. Mater. Chem.* **2011**, *21*, 16819.
[13] M. Llusar, V. Royo, J. A. Badenes, M. A. Tena, G. Monrós, *Journal of the European Ceramic Society* **2009**, *29*, 3319.
[14] I. T. Papadas, S. Fountoulaki, I. N. Lykakis, G. S. Armatas, *Chem. Eur. J.* **2016**, *22*, 4600.
[15] P. Li, D. E. Miser, S. Rabiei, R. T. Yadav, M. R. Hajaligol, *Applied Catalysis B: Environmental* **2003**, *43*, 151.
[16] S. T. Navale, D. K. Bandgar, S. R. Nalage, G. D. Khuspe, M. A. Chougule, Y. D. Kolekar, S. Sen, V. B. Patil, *Ceramics International* **2013**, *39*, 6453.
[17] Z. Ai, K. Deng, Q. Wan, L. Zhang, S. Lee, *J. Phys. Chem. C* **2010**, *114*, 6237.
[18] P. J. Borm, D. Robbins, S. Haubold, T. Kuhlbusch, H. Fissan, K. Donaldson, R. Schins, V. Stone, W. Kreyling, J. Lademann, J. Krutmann, D. Warheit, E. Oberdorster, *Part Fibre Toxicol* **2006**, *3*, 11.
[19] A. Sánchez, S. Recillas, X. Font, E. Casals, E. González, V. Puntes, *TrAC Trends in Analytical Chemistry* **2011**, *30*, 507.
[20] L. M. A. Ali, M. Gutiérrez, R. Cornudella, J. A. Moreno, R. Piñol, L. Gabilondo, A. Millán, F. Palacio, *J Biomed Nanotechnol* **2013**, *9*, 1272.
[21] M.-T. Zhu, W.-Y. Feng, B. Wang, T.-C. Wang, Y.-Q. Gu, M. Wang, Y. Wang, H. Ouyang, Y.-L. Zhao, Z.-F. Chai, *Toxicology* **2008**, *247*, 102.
[22] U. Sakulkhu, L. Maurizi, M. Mahmoudi, M. Motazacker, M. Vries, A. Gramoun, M.-G. Ollivier Beuzelin, J.-P. Vallée, F. Rezaee, H. Hofmann, *Nanoscale* **2014**, *6*, 11439.
[23] C. Vogt, M. Pernemalm, P. Kohonen, S. Laurent, K. Hultenby, M. Vahter, J. Lehtiö, M. S. Toprak, B. Fadeel, *PLoS ONE* **2015**, *10*, e0129008.
[24] G. Stepien, M. Moros, M. Pérez-Hernández, M. Monge, L. Gutiérrez, R. M. Fratila, M. de las Heras, S. Menao Guillén, J. J. Puente Lanzarote, C. Solans, J. Pardo, J. M. de la Fuente, *ACS Appl. Mater. Interfaces* **2018**, *10*, 4548.
[25] H. Arami, A. Khandhar, D. Liggitt, K. M. Krishnan, *Chem Soc Rev* **2015**, *44*, 8576.

[26] Q. Feng, Y. Liu, J. Huang, K. Chen, J. Huang, K. Xiao, *Sci Rep* **2018**, *8*, 2082.
[27] M. A. Dobrovolskaia, A. K. Patri, J. Zheng, J. D. Clogston, N. Ayub, P. Aggarwal, B. W. Neun, J. B. Hall, S. E. McNeil, *Nanomedicine* **2009**, *5*, 106.
[28] A. Solorio-Rodríguez, V. Escamilla-Rivera, M. Uribe-Ramírez, A. Chagolla, R. Winkler, C. M. García-Cuellar, A. De Vizcaya-Ruiz, *Nanoscale* **2017**, *9*, 13651.
[29] U. Sakulkhu, M. Mahmoudi, L. Maurizi, J. Salaklang, H. Hofmann, *Sci Rep* **2014**, *4*, 5020.
[30] U. Sakulkhu, M. Mahmoudi, L. Maurizi, G. Coullerez, M. Hofmann-Amtenbrink, M. Vries, M. Motazacker, F. Rezaee, H. Hofmann, *Biomater Sci* **2015**, *3*, 265.
[31] H. Zhang, P. Wu, Z. Zhu, Y. Wang, *Spectrochim Acta A Mol Biomol Spectrosc* **2015**, *151*, 40.
[32] V. Hirsch, C. Kinnear, M. Moniatte, B. Rothen-Rutishauser, M. J. D. Clift, A. Fink, *Nanoscale* **2013**, *5*, 3723.
[33] D. Khang, Y. K. Lee, E.-J. Choi, T. J. Webster, S.-H. Kim, *IJN* **2014**, 97.
[34] A. Nemmar, S. Beegam, P. Yuvaraju, J. Yasin, S. Tariq, S. Attoub, B. H. Ali, *Part Fibre Toxicol* **2016**, *13*, 22.
[35] I. K. Herrmann, M. Urner, M. Hasler, B. Roth-Z'Graggen, C. Aemisegger, W. Baulig, E. K. Athanassiou, S. Regenass, W. J. Stark, B. Beck-Schimmer, *Nanomedicine (Lond)* **2011**, *6*, 1199.
[36] T. Liu, R. Bai, H. Zhou, R. Wang, J. Liu, Y. Zhao, C. Chen, *RSC Adv.* **2020**, *10*, 7559.
[37] In *Platelets*, Academic Press, **2013**.
[38] J. T. Vivian, P. R. Callis, *Biophysical Journal* **2001**, *80*, 2093.
[39] M. Möller, A. Denicola, *Biochem. Mol. Biol. Educ.* **2002**, *30*, 309.
[40] C. Hao, G. Xu, Y. Feng, L. Lu, W. Sun, R. Sun, *Spectrochimica Acta Part A: Molecular and Biomolecular Spectroscopy* **2017**, *184*, 191.
[41] M. Chastellain, A. Petri, H. Hofmann, *Journal of Colloid and Interface Science* **2004**, *278*, 353.
[42] A. Petri-Fink, M. Chastellain, L. Juillerat-Jeanneret, A. Ferrari, H. Hofmann, *Biomaterials* **2005**, *26*, 2685.
[43] L. Maurizi, U. Sakulkhu, L. A. Crowe, V. M. Dao, N. Leclaire, J.-P. Vallée, H. Hofmann, *RSC Adv.* **2014**, *4*, 11142.
[44] L. Ma, F. Yang, J. Zheng, *Journal of Molecular Structure* **2014**, *1077*, 87.
[45] H. Derakhshankhah, A. Hosseini, F. Taghavi, S. Jafari, A. Lotfabadi, M. R. Ejtehadi, S. Shahbazi, A. Fattahi, A. Ghasemi, E. Barzegari, M. Evini, A. A. Saboury, S. M. K. Shahri, B. Ghaemi, E.-P. Ng, H. Awala, F. Omrani, I. Nabipour, M. Raoufi, R. Dinarvand, K. Shahpasand, S. Mintova, M. J. Hajipour, M. Mahmoudi, *Sci Rep* **2019**, *9*, 1558.
[46] B. Kharazian, S. E. Lohse, F. Ghasemi, M. Raoufi, A. A. Saei, F. Hashemi, F. Farvadi, R. Alimohamadi, S. A. Jalali, M. A. Shokrgozar, N. L. Hadipour, M. R. Ejtehadi, M. Mahmoudi, *Sci Rep* **2018**, *8*, 12557.
[47] J. Deng, M. Sun, J. Zhu, C. Gao, *Nanoscale* **2013**, *5*, 8130.
[48] Z. J. Deng, M. Liang, M. Monteiro, I. Toth, R. F. Minchin, *Nat Nanotechnol* **2011**, *6*, 39.
[49] R. M. Visalakshan, A. A. Cavallaro, M. N. MacGregor, E. P. Lawrence, K. Koynov, J. D. Hayball, K. Vasilev, *Advanced Functional Materials* **2019**, *29*, 1970088.
[50] S. Shrivastava, S. K. Singh, A. Mukhopadhyay, A. S. K. Sinha, R. K. Mandal, D. Dash, *Colloids Surf B Biointerfaces* **2011**, *82*, 241.
[51] C. Strehl, T. Gaber, L. Maurizi, M. Hahne, R. Rauch, P. Hoff, T. Häupl, M. Hofmann-Amtenbrink, A. R. Poole, H. Hofmann, F. Buttgereit, *Int J Nanomedicine* **2015**, *10*, 3429.
[52] M. Bardhan, G. Mandal, T. Ganguly, *Journal of Applied Physics* **2009**, *106*, 034701.
[53] C. W. Fuller, J. N. Miller, *Proc. Anal Div. Chem.Soc* **1979**, *16*, 199.

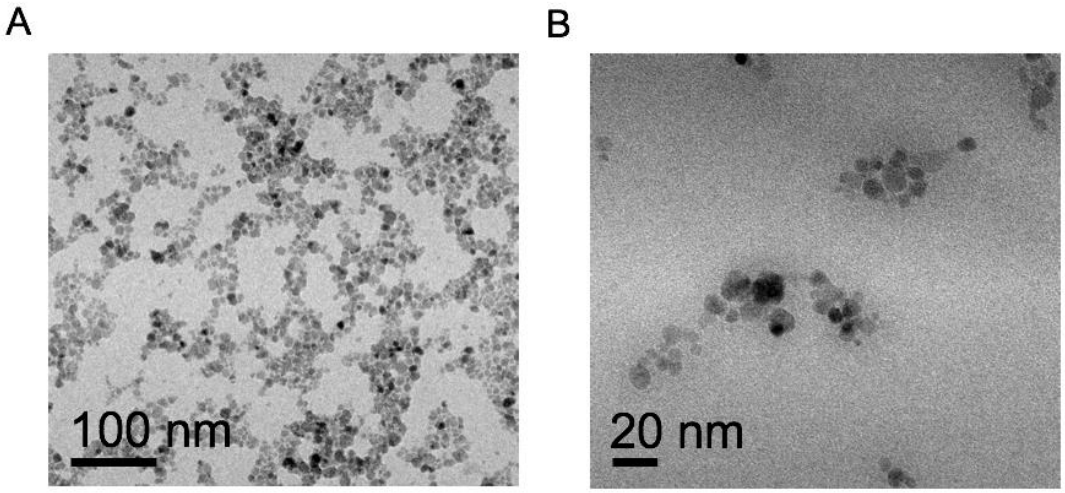

Figure 1. Transmission electron micrographs of the bare SPIONs.

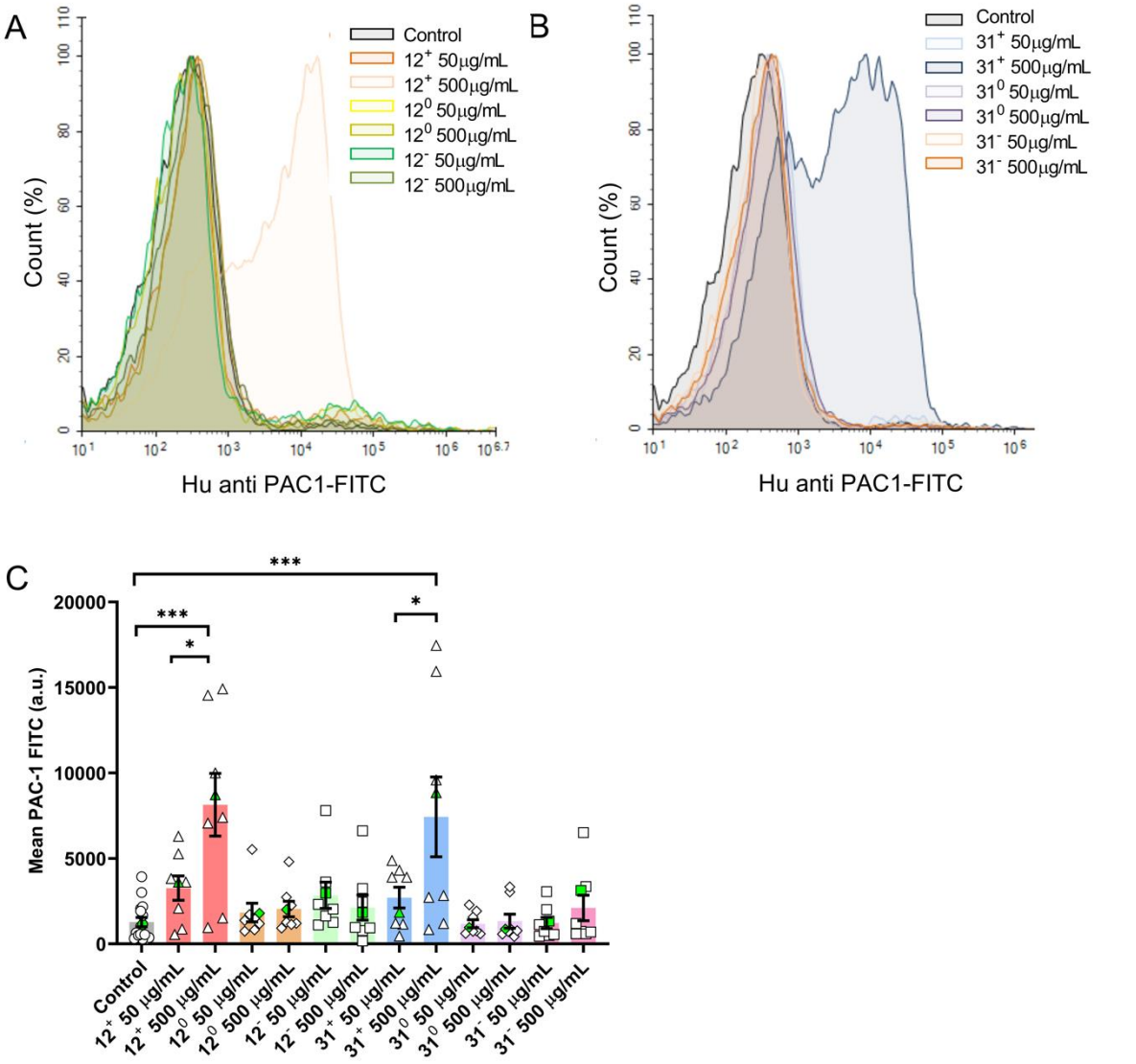

Figure 2. Effect of PVA-SPIONs on platelet activation in absence of platelet agonist. Representative histograms of platelet activation (FITC-conjugated PAC-1 antibody binding activated GPIIb-IIIa) in presence of (A) 12 kDa PVA-coated SPIONs and (B) 31 kDa PVA-coated SPIONs with resulting positive (+), neutral (0) or negative (-) surface charge. (C) Corresponding quantification of platelet activation following platelet incubation with 12 kDa and 31 kDa PVA-coated SPIONs (n=8, 4 donors, *P<0.05, ***P≤0.001). The green symbols highlight the datapoints selected for the representative histograms A and B.

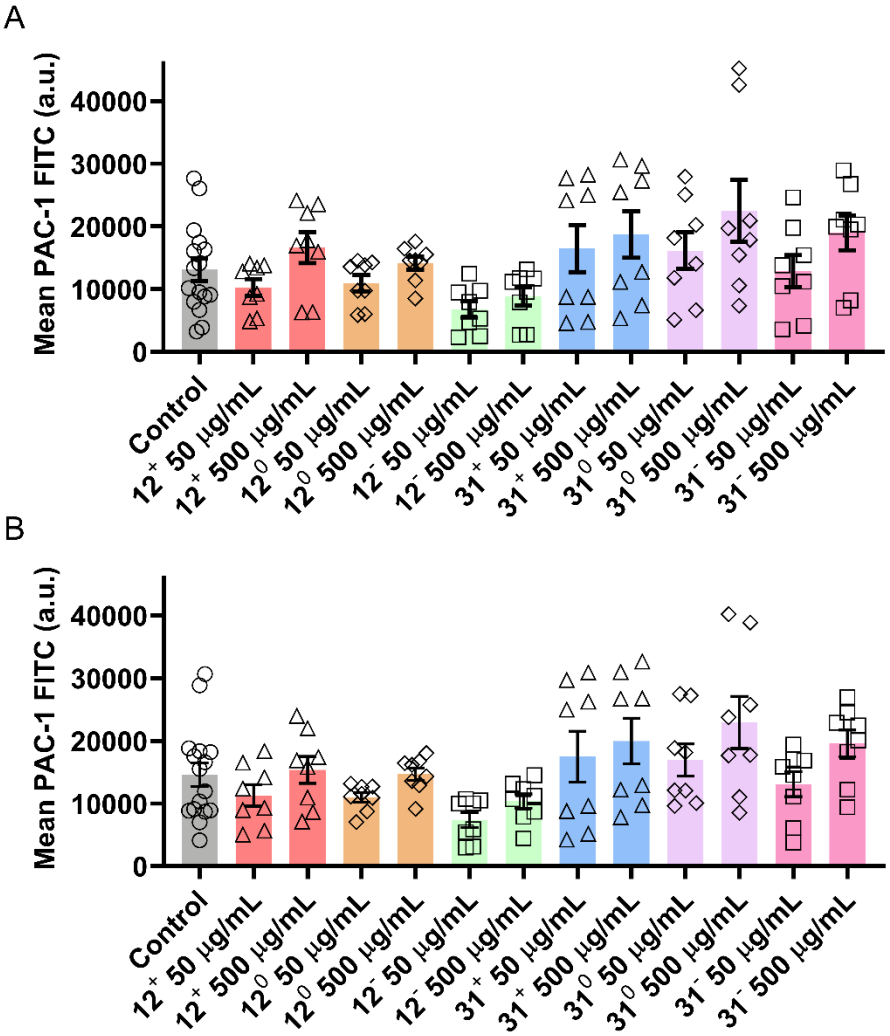

Figure 3. Effect of PVA-SPIONs on platelet activation in the presence of platelet agonist. Platelet activation as measured by FITC-conjugated PAC-1 antibody binding, in presence of 12 kDa and 31 kDa PVA-coated SPIONs along with ADP (A) 20 µM and (B) 50 µM (n=8, 4 donors, P = ns (non-significant) for all conditions).

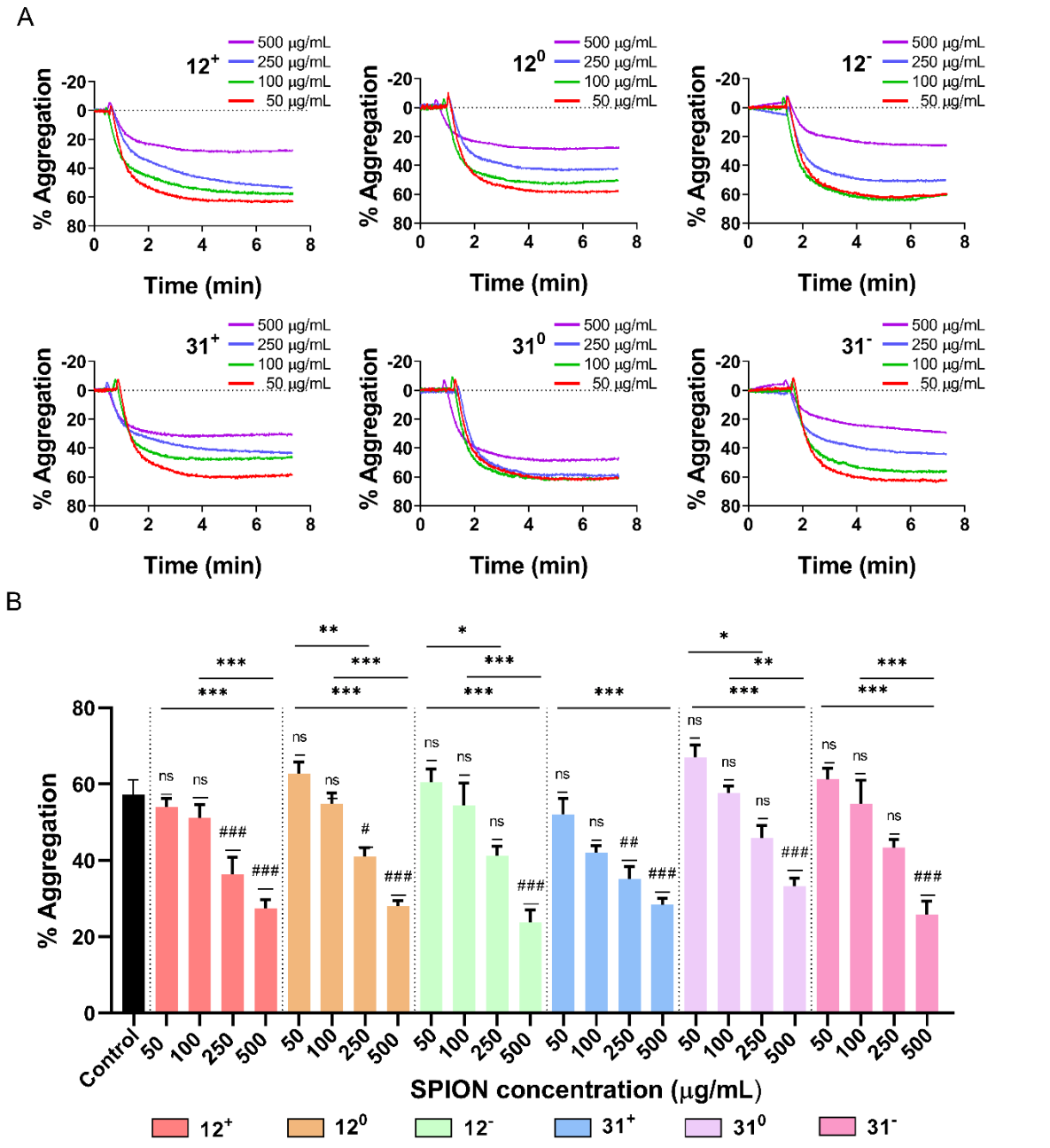

Figure 4. Influence of PVA-SPIONs on ADP-induced platelet aggregation in plasma. (A) Representative LTA aggregation curves and (B) quantification of platelet aggregation in the presence of varying concentrations of 12 kDa and 31 kDa PVA-coated SPIONs with resulting positive (+), neutral (0) or negative (-) surface charge (n=6 to 18, 3 to 9 donors, $^{\#}P\leq0.05$, $^{\#\#}P\leq0.01$, $^{\#\#\#}P\leq0.001$, *P≤0.05, **P≤0.01, ***P≤0.001). ADP 20 µM was used as platelet agonist, including in the control samples. # symbol denotes significance compared to the control group.

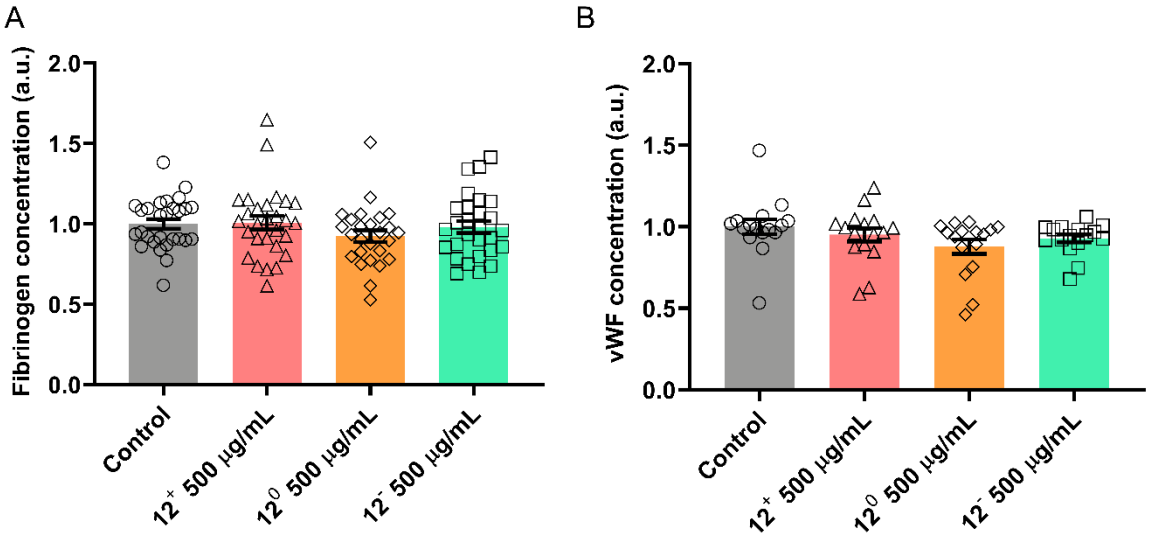

Figure 5. Effect of PVA-SPIONs on plasma fibrinogen and vWF levels. Quantification of (A) fibrinogen and (B) vWF using ELISAs in plasma from various donors following its incubation with PVA-coated SPIONs (n=28, 14 donors, and n=16 and 8 donors, respectively, P = ns for all conditions).

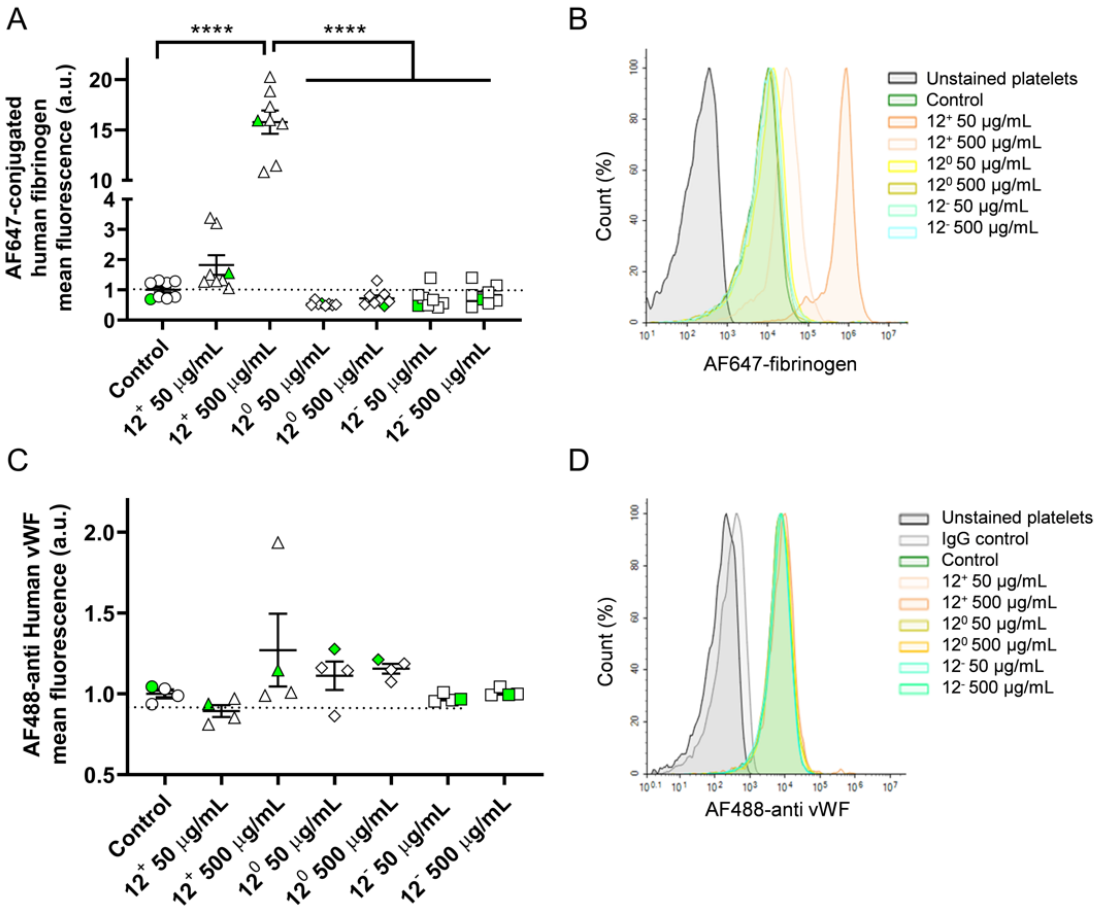

Figure 6. Assessment of the steric effect of PVA-SPIONs on fibrinogen and vWF. Quantification and representative flow cytometry histograms of (A-B) FITC-conjugated fibrinogen (n=8, 4 donors, **** P<0.0001) and (C-D) anti-human-vWF antibody to GPIIb-IIIa (n=4, 2 donors, P = ns for all conditions). The green symbols highlight the datapoints selected for the representative histograms B and D.

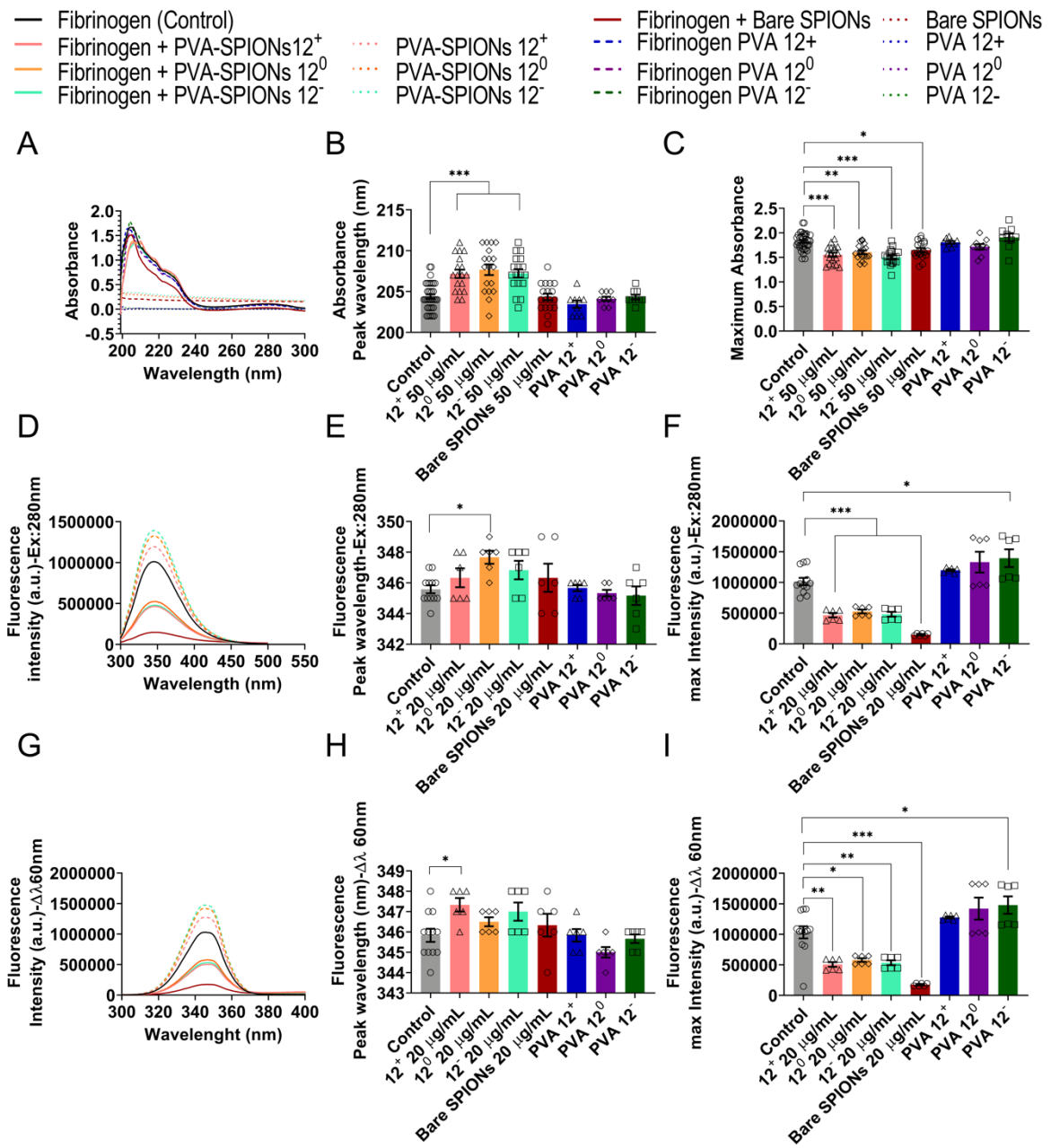

Figure 7. Effect of PVA-SPIONs on fibrinogen conformation. (A) Representative absorbance curves of fibrinogen in the presence or absence of PVA-coated SPIONs, bare SPIONs and PVA, (B) Quantification of fibrinogen maximum absorbance peak (n=9 to 36, ***P≤0.001), (C) Quantification of peak absorbance wavelength (n=9 to 36, *P≤0.05, **P≤0.01, ***P≤0.001). (D-F) Intrinsic tryptophan and tyrosine fluorescence measured in steady state (Ex = 280 nm) and (G-I) intrinsic tryptophan fluorescence measured synchronous fluorescence with **Δ**λ = 60 nm. Data display (D,G) the representative spectra, (E,H) histograms of the λ_{max} (n=6 to 12, *P<0.05) and (F,I) histograms of the maximum intensity for each conditions (n=6 to 12, *P<0.05, **P<0.01, ***P<0.001).

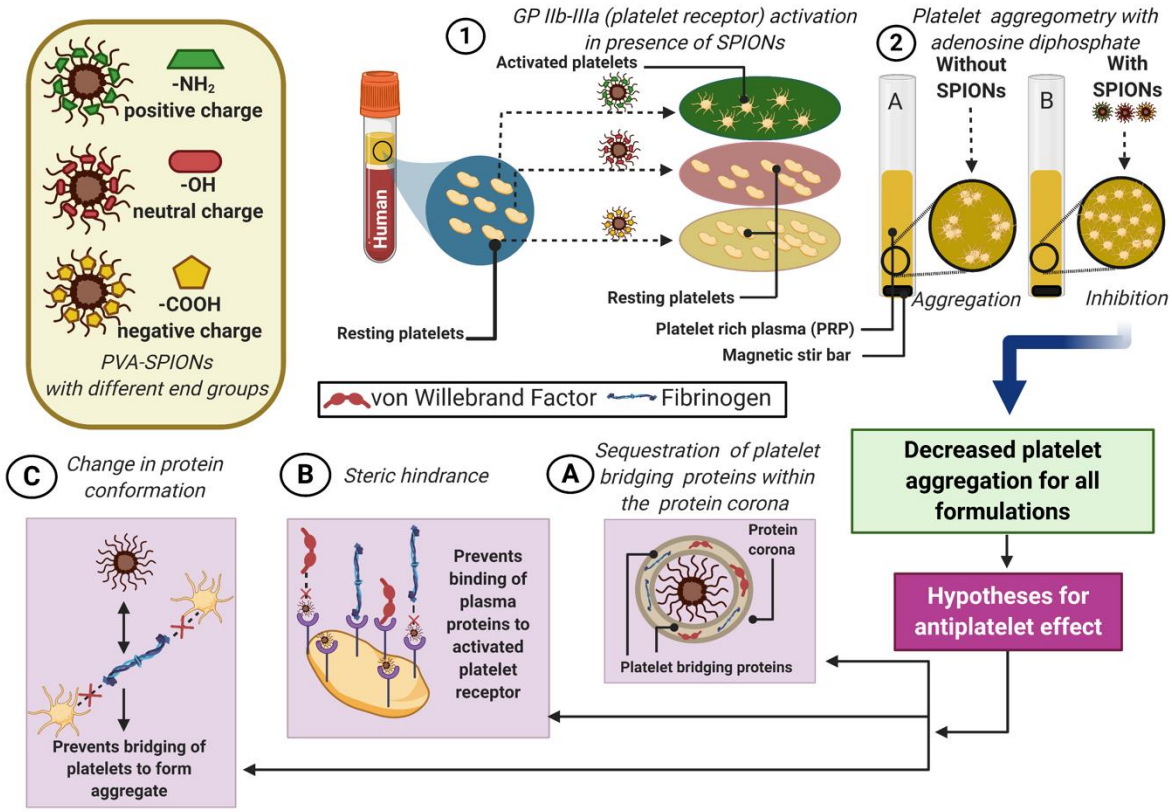

Figure 8. Scheme summarizing the key findings and tested hypotheses to explain the observed anti-platelet effect induced by PVA-SPIONs.

Table 1. Formulation and characterization of PVA-coated SPION suspensions

Suspensions	**Bare SPIONs**	**12^-**	**31^-**	**12^0**	**31^0**	**12^+**	**31^+**
Polymer types	N/A	PVA-12 PVA-COOH	PVA-31 PVA-COOH	PVA-12	PVA-31	PVA-12 PVA-NH_2	PVA-31 PVA-NH_2
Mass ratios (SPIONs/PVA_1/PVA_2)	N/A	1/4.5/4.5	1/4.5/4.5	1/9	1/9	1/9/0.2	1/9/0.2
End groups (SPION surface)	OH	OH/COOH	OH/COOH	OH	OH	OH/NH_2	OH/NH_2
Size[a] (nm)	23 (± 7)* 1930 (± 27)	80 (± 27)	88 (± 30)	72 (± 22)	68 (± 22)	87 (± 37)	83 (± 29)
Zeta potential[b] (mV)	0	-6 (± 1)	-4 (± 1)	0	0	+7 (± 1)	+12 (± 1)

[a)]Number weighted, 150 mM NaCl, pH 7.4; [b)] 10 mM NaCl, pH 7.4; * value measured at pH 4, NaCl 10 mM.

The interactions and effects of superparamagnetic iron oxide nanoparticles (SPIONs) on human platelets are being assessed *ex vivo*. SPIONs induce a significant antiplatelet effect independent of the surface chemistry of the nanoparticles. This effect correlates with a SPION-induced change in conformation of fibrinogen, an essential plasma protein responsible for bridging platelets during hemostasis.

Anti-platelet effect induced by iron oxide nanoparticles: correlation with conformational change in fibrinogen

Regina Komal Kottana, Lionel Maurizi, Brian Schnoor, Kenise Morris, Jessica Ann Webb, Michael Anthony Massiah, Nadine Millot, Anne-Laure Papa*

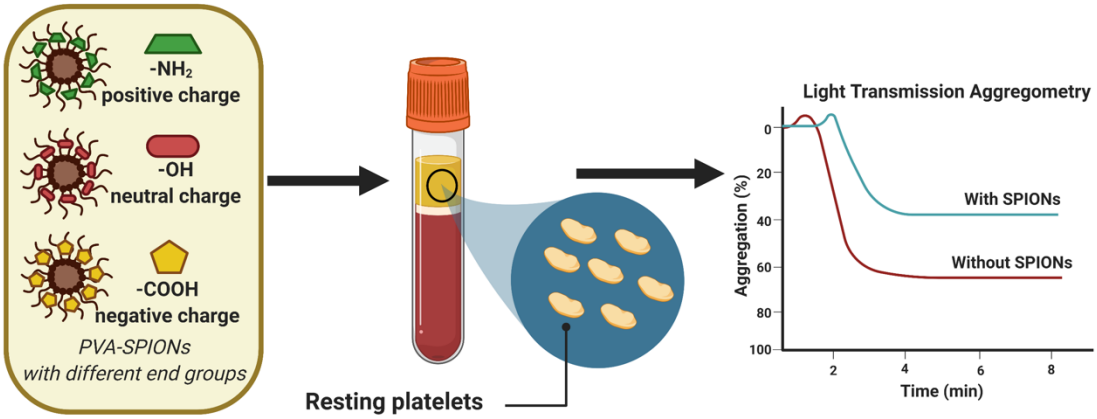

Supporting Information

Anti-platelet effect induced by iron oxide nanoparticles: correlation with conformational change in fibrinogen

Regina Komal Kottana, Lionel Maurizi, Brian Schnoor, Kenise Morris, Jessica Ann Webb, Michael Anthony Massiah, Nadine Millot, Anne-Laure Papa*

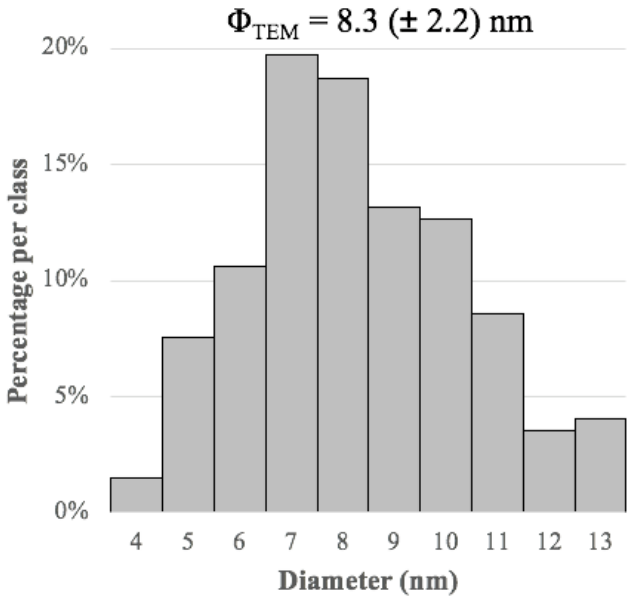

Figure S1. Diameter distribution of 200 bare SPIONs and average diameter (Φ_{TEM}) as measured on transmission electron micrographs.

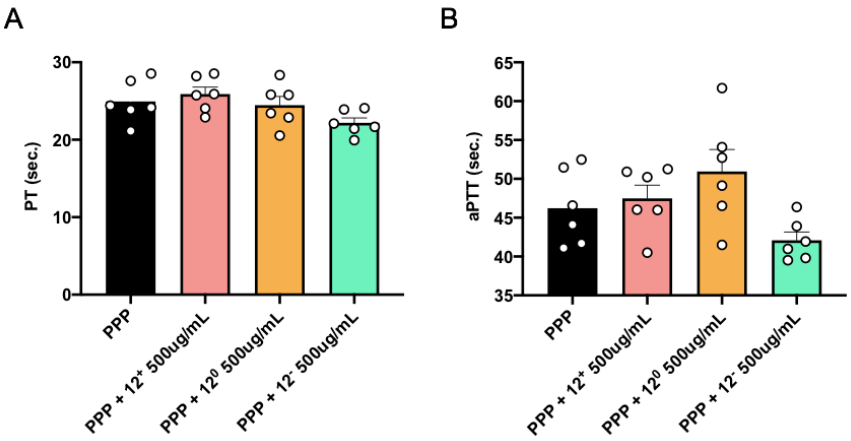

Figure S2. (A) Prothrombin time (PT) and (B) activated partial thromboplastin time (aPTT) of human platelet poor plasma (PPP) samples with/without PVA-SPIONs (n=6).

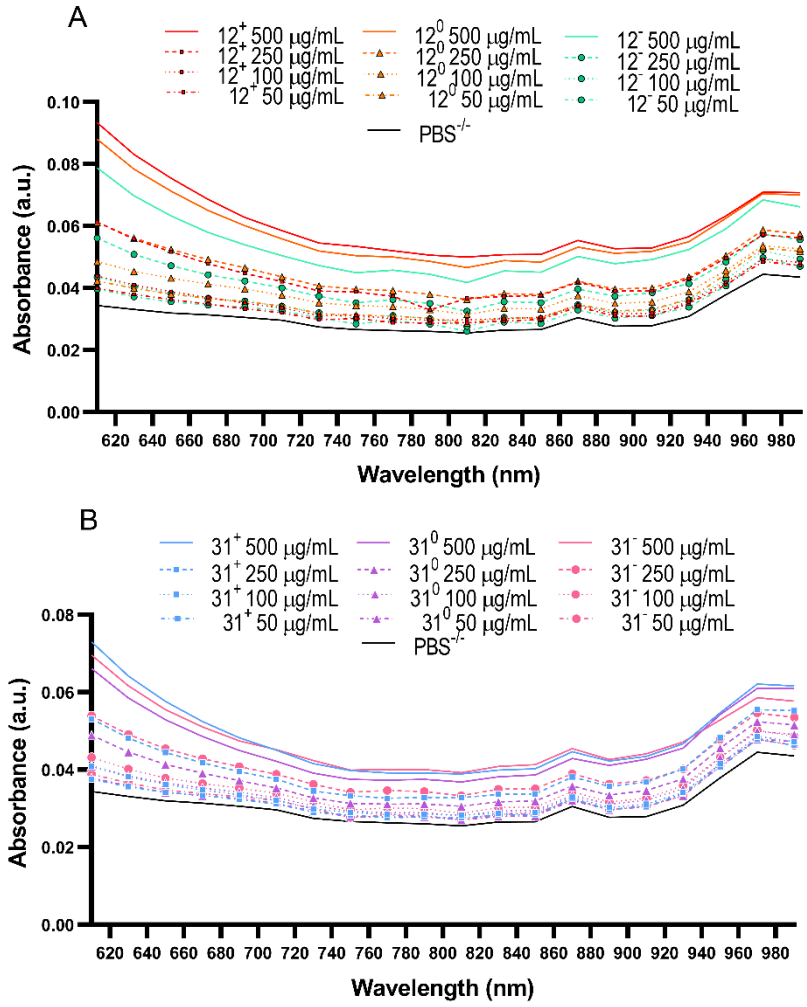

Figure S3. Absorbance curves of the PVA-coated SPIONs with PVA (A) 12 kDa and (B) 31 kDa, and with resulting positive (+), neutral (0) or negative (-) surface charge (n=6)**.**

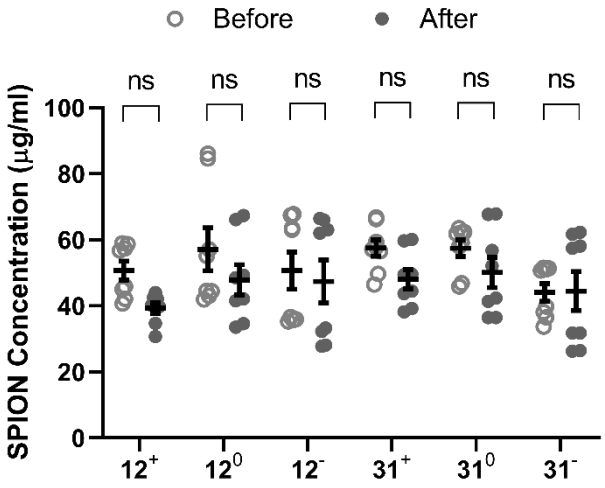

Figure S4. Particle concentration in sample suspensions before and after LTA measurements. Iron detected in suspensions of PBS by ferrozine assay before and after incubation with the various PVA-SPION formulations in the aggregometer (n=8).